Photocatalytic degradation of ciprofloxacin drug utilizing novel PVDF/polyaniline/lanthanum strontium manganate@Ag composites

Swayam Aryam BEHERA[1], Ali AMANAT[2], P. Ganga Raju ACHARY[1,*]

[1] Department of Chemistry, Faculty of Engineering and Technology (ITER), Siksha 'O' Anusandhan, Deemed to be university, Bhubaneswar, Odisha, 751030, India
[2] Department of New Materials and Nanotechnology, National University of Science and Technology MISiS, Moscow, Russia

*Corresponding author e-mail: pgrachary@soa.ac.in

Abstract

Poly (vinylidene fluoride) (PVDF) is the first-choice ferroelectric support or membrane material. The lanthanum strontium manganite (LSMO) is a well-known electrode material in the class of the solid oxide fuel cell (SOFC) materials. A set of four polymer composites PVDF-LSMO-PANI(5.0 wt%) with different amount of silver doping were fabricated with the silver nitrate and reducing agent. The characterization of these four novel PVDF based composites were characterized by the XRD, FTIR, SEM, UV-Visible DRS. The present communication highlights: (I) the effect of PANI in the PVDF-LSMO-PANI (PLP) composites towards the photocatalytic degradation of ciprofloxacin drug. (II) the effect of Ag doping in the Ag-PVDF-LSMO-PANI (Ag-PLP) composites towards the photocatalytic degradation of ciprofloxacin drug. It is observed that the incorporation of PANI in PVDF-LSMO and Ag in PVDF-LSMO-PANI polymer ceramic composites showed enhanced photocatalytic degradation of ciprofloxacin in the irradiation of visible radiation. The plausible separation of photo-generated e⁻ hole pairs (e^- and h^+) carried on by charge migration kind of mechanism is being studied here to understand the improved photocatalytic activity of Ag-PVDF-LSMO-PANI composites.

1. Introduction

A specific type of friendly and green technology that is better for the sustainable growth of the environment is photocatalytic technology, which is utilised to degrade organic pollutants and convert solar energy to solve environmental issues and energy crises. As a result, it brought about more and more interest in research. Different photocatalyst, such as metallic sulphide, metallic oxide, metallic semiconductors, non-metallic semiconductors have been developed and extensively explored, particularly for the degradation of pollutants, heavy metals, water splitting etc [1-5]. The photocatalysts having silver doping are capturing greater interest among these many types of photocatalyst because of their photosensitivity to visible light, which might optimise solar energy and improve photocatalytic activity [6].

PVDF polymer is so flexible that, it can be formed easily on curved surfaces, giving it a distinct advantage over ceramic. Additionally, it is tough, creep-resistant, chemically inert and has good stability when exposed to sunlight. The addition of piezoceramics to a PVDF matrix [7-9] has been tried to enhance the photocatalytic activity. However, design and fabrication complexity, environmentally friendly and cost always remained issues. The improved adsorption capabilities and catalytic performance of PVDF composites, in contrast to pure PVDF, stem from surface modifications, synergistic effects, heightened porosity, and the capacity to customize material properties through the incorporation of diverse fillers. These advancements render PVDF composites appealing for diverse applications, spanning environmental remediation and photocatalysis.

The silver compounds have characteristics with plasma, photosensitivity and small band gap that make them simple to activate in visible light and exhibit potential photocatalytic activity. The most promising organic conducting polymer is polyaniline (PANI), which is used in applications like molecular sensors, gas separation membranes, rechargeable batteries, and metal corrosion protection [10]. PANI is a pH-responsive material that, when subjected to acid/base treatment, takes on various chemical forms. PANI, however, exhibits poor mechanical properties because of its poor solubility in common organic solvents [11]. Numerous studies have been conducted on the use of additives and/ or particular dopants for PANI composites to address these drawbacks. The PANI composite can therefore be attributed with particular properties, such as conducting and mechanical properties and superior solvent solubility [12], which could lead to increased photocatalytic property. Nobel metal silver doping significantly enhances the thermal, photocatalytic activity of PANI. Hence, the mixture of PANI and silver with homogeneous dispersion improved photocatalytic activity of the functional composite materials.

Due to the long-lasting adverse effects, organic pollutants have a significant effect on water. Among the various kinds of organic pollutants, hormone disrupting substances like petroleum, dyes, and pharmaceutical ingredients are extremely hazardous for aquatic life, people and vegetation. Antimicrobial drugs like antibiotics are currently

used extensively to kill or halt the growth of bacteria. Antimicrobial medications come in a wide variety of forms with various structures and purposes [13]. Ciprofloxacin (CIP) is a class of antimicrobial medication used primarily by people for the treatment of joint infection, gram positive, gram negative, and typhoid illness. Additionally, because of their extensive utilization, it has been found in surface water, ground water, drinking water, and sewage water [14]. Furthermore, when the aforementioned waters are used to irrigate agricultural territory, these antibiotics are frequently found in the soil. Therefore, the CIP deterioration can be resolved using a variety of conventional methods, including electrochemistry, bacteria decomposition, adsorption technology. In light of these techniques, semiconductor photocatalytic technology has received a lot of attention from academics as an effective and environmentally friendly way to degrade environmental pollutants[15].

In the present communication, the Ag-PVDF-LSMO-PANI (Ag-PLP) composite polymer films are fabricated by solution casting method. The structural and morphological study along with optical characteristics are obtained by SEM, FT-IR and UV- DRS. The Ag-PLP composite has demonstrated excellent photocatalytic properties, making it an effective material for the degradation of ciprofloxacin drugs in wastewater treatment. The impact of this material lies in its potential to address the growing concern of antibiotic resistance and environmental pollution caused by the improper disposal of pharmaceutical drugs. These materials shown great promise in degrading ciprofloxacin efficiently, offering an effective solution to this issue. The photocatalytic properties of the Ag-PLP composite material allow it to degrade ciprofloxacin under visible light, which is a significant advantage over other photocatalysts that require UV light.

2. Experimental details

2.1 Materials

The dimethyl formamide (DMF) having 99% purity was brought from Merck and poly vinylidene fluoride (PVDF) pellet was purchased from HI Media laboratories. Manganese acetate [Mn $(CH_3CO_2)_2$], Strontium nitrate [$Sr(NO_3)_2$] and Lanthanum nitrate [$La(NO_3)_3$] were from HI Media laboratories. The ammonium persulfate (APS) and aniline were purchased from Merck.

Synthesis of Lanthanum Strontium Manganese Oxide (LSMO) is described in our previous publication [16]. A combination of ammonium persulfate (APS) as initiator and chemical oxidative polymerization of aniline monomer, polyaniline (PANI) was synthesized by maintaining the flow rate and stirring for 6 h at room temperature. After the polymerization reaction, the resultant mixture was filtered and washed successively using 1.0 M HCl several times followed by double distilled water until the washing became colourless. Finally, using acetone, the residue was washed and dried at 60°C.

2.2 PVDF/LSMO/PANI@Ag (Ag-PLP)

A set of four polymer composites PVDF-LSMO-PANI (5.0 wt%) with different weight percentage (2.5, 5.0, 7.5, and 10.0 wt%) of silver doping were fabricated with the silver nitrate ($AgNO_3$) and reducing agent ($NaBH_4$) and named as Ag-PLP-2.5%, Ag-PLP-5.0%, Ag-PLP-7.5% and Ag-PLP-10.0%.

For the polymer sheet fabrication Ag-PLPs materials were taken individually in glass beakers according to their stoichiometric proportions. About 50 mL of Dimethyl formamide (DMF) solvent was gradually poured into it and stirred continuously with constant heating (approx. 80°C) on a hot plate till a homogeneous solution was obtained. Then the mixtures were poured into petri dishes and placed at room temperature till the evaporation of excess DMF. After the complete evaporation of the solvent, the polymer sheets were peeled out from the petri dishes and labelled for further characterizations. The schematic representation of synthesis of LSMO, PANI and polymer sheet fabrication is illustrated in Figure 1.
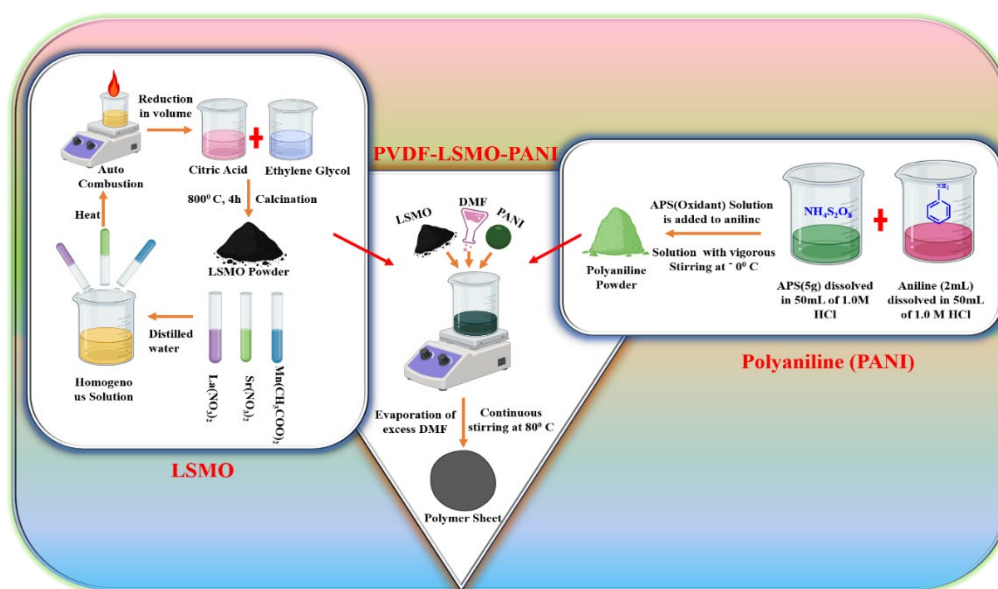

Figure 1. Schematic representation for synthesis of polymer sheet fabrication

3. Results and discussion

3.1 FTIR Analysis

The structural analysis of PLP, Ag-PLP and Pure PVDF was performed by FTIR spectrum using Jasco FT/IR-4600 (Model no. FT/IR-4600LE) and shown in Figure 2(a) and Figure 2(b) respectively. For polyaniline, the IR band specific to C-H vibrations (2965, 2931, 2842, 1375, 994, 970, and 910 cm^{-1}), N-H vibrations (3370, 3200, and 3023 cm^{-1}), C-N vibration (1650 cm^{-1}), C=C vibrations (1595, 1510, 1495, and 1450 cm^{-1}), C-N vibration (1312 cm^{-1}) are observed [17-21]. Bands at 2956.21 cm^{-1} and 2880.57 cm^{-1} region arising from C-H stretching. The main absorption band at 615 cm^{-1} is caused by the perovskite's metal oxygen bond being stretched. Within the MnO$_6$ octahedral structure, the Mn-O-Mn bond length is altered by this internal motion. Carbonates is indicated around 920 cm^{-1} and 1050 cm^{-1} by the absorption peaks. The stretching vibration of carboxylic group (COO-) in carbonate is revealed by the strong absorption peak around 1381 cm^{-1} in LSMO. O-C-O is responsible for the absorption peak at 2360 cm^{-1}. The characteristic of absorbed water or the -OH group in the alcohol is the broad absorption peak around 3350 cm^{-1}. The Mn-O-Mn bond length changes in the stretching, whereas the Mn-O-Mn bond angle changes in the stretching mode. According to transmission spectra, the structure of LSMO has formed, which is consistent with the XRD findings. This is shown by the appearance of stretching and bending modes.

The proportion of β-phase present in the material can potentially be determined employing a method described by Gregorio [22]. For each phase the, the following formula (Equation (1)) applies for a film sample with thickness of 'L' and IR absorption bands:

$$A = log\ (I_o/I)\ =\ \mathcal{E}.X.L \tag{1}$$

where, I: incident, I$_0$: transmitted radiation intensities, $\mathcal{E}$: extinction co-efficient of IR bands corresponding to each phase (6.1×10^4 cm^2·mol^{-1} for α and 7.7×10^4 cm^2·mol^{-1} for β-phase), and X: degree of crystallinity of each phase. Therefore, percentage of F(β), the relative fraction of β-phase, in the material with α and β-phases, can be expressed using Equation (2):

$$\%F(\beta) = \left[\frac{X_\beta}{X_\alpha + X_\beta}\right] \times 100 = \left[\frac{A_\beta}{1.26A_\alpha + A_\beta}\right] \times 100 \tag{2}$$

The A$_\alpha$ and A$_\beta$ correspond to absorption bands at 530 cm^{-1} and 840 cm^{-1} for α and β-phases, respectively. The value of F(β) obtained for the Ag-PLP and Pure PVDF at 840 cm^{-1} was 52% and 57% respectively.

3.2 SEM

The morphological study of composite sheets obtained by ZEISS (EVO 18) scanning electron microscope. Figure 3(a) and Figure 3(b) represents the microstructure of PLP 7.5 wt% and Ag-PLP 7.5 wt% polymer sheet with particle size distribution respectively. The figure suggest that there is no clustering of particles. The mean value of the size of nanoparticles of PLP is 2.29 μm with std. deviation 1.12 and Ag-PLP systems is 2.85 μm with std. deviation 0.62. The EDS spectra shows that all the elements are present without any trace of impurity. Figure 3(c) shows EDS spectra colour maping of Ag-PLP 7.5 wt% system in which the presence of elements are clearly visible.

3.3 UV-DRS

The analysis of UV-Visible spectra broadens the responsiveness of the sample to electromagnetic radiations and increases its potential for application. The energy of incident photon and absorbance having relationship is shown in Equation (3):

$$(\alpha h\upsilon)^2 = C(h\upsilon - E_g) \tag{3}$$

Where α is absorption coefficient, h is plank's constant, υ is the incoming light frequency, A is the absorption coefficient, E$_g$ is the band gap and C donates absorption constant. The band gap energy of the developed photocatalyst can be determined by plotting $(\alpha h\upsilon)^2$ for direct transition against energy. The absorbance spectrum of PVDF and Ag-PLP 7.5 wt% is shown in Figure 4(a), the energy band gap is shown in Figure 4(b) and the value of E$_g$ are determined by the X-axis intercept. The calculated value of $(\alpha h\upsilon)^2$ vs hυ provides the direct allowed bandgap energy of 4.66 eV for PVDF and 2.60 eV for Ag-PLP 7.5 wt% [23,24]. As observed, Ag-PLP 7.5 wt% have lower band gap energy which makes it useful for photocatalytic and electrical application.
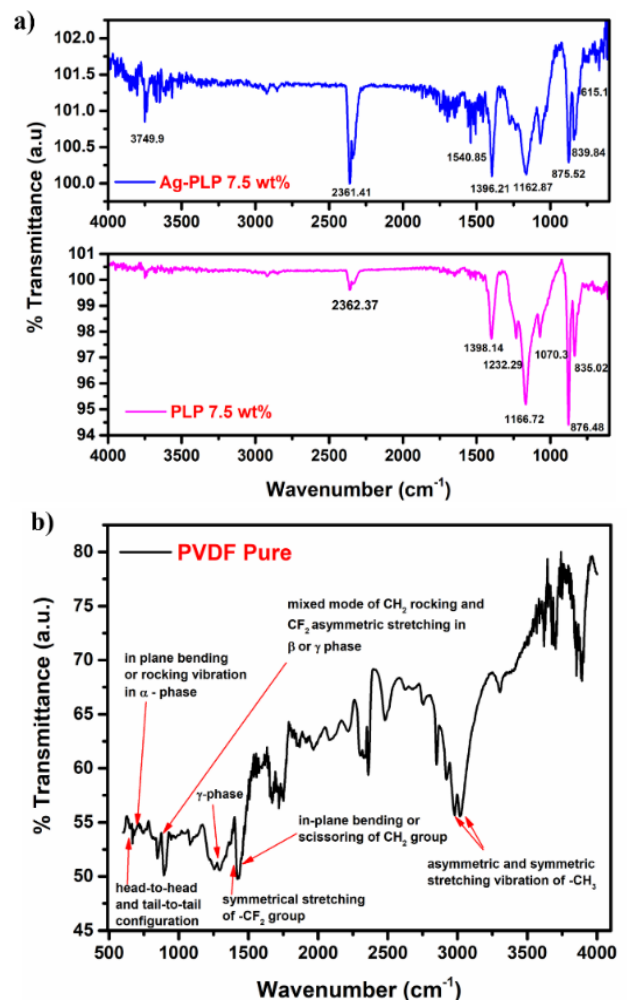

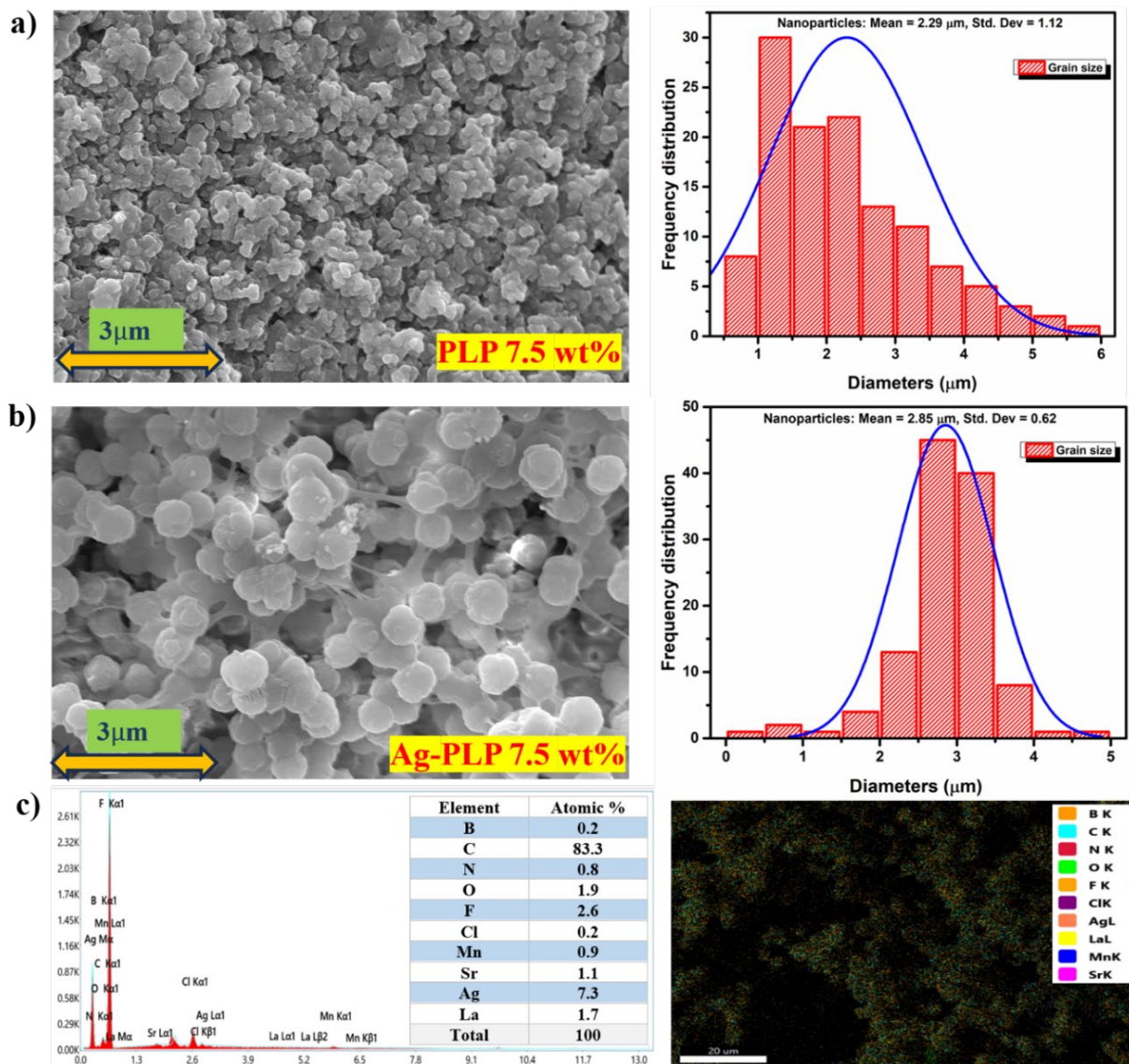**Figure 2.** (a) FTIR spectra of PLP and Ag-PLP and (b) FTIR spectra of Pure PVDF.

Figure 3. (a) Surface micrograph with particle size distribution of PLP 7.5 wt% (b) Surface micrograph with particle size distribution of Ag-PLP 7.5 wt%, and (c) EDS spectra of Ag-PLP 7.5 wt% with colour maping of various elements
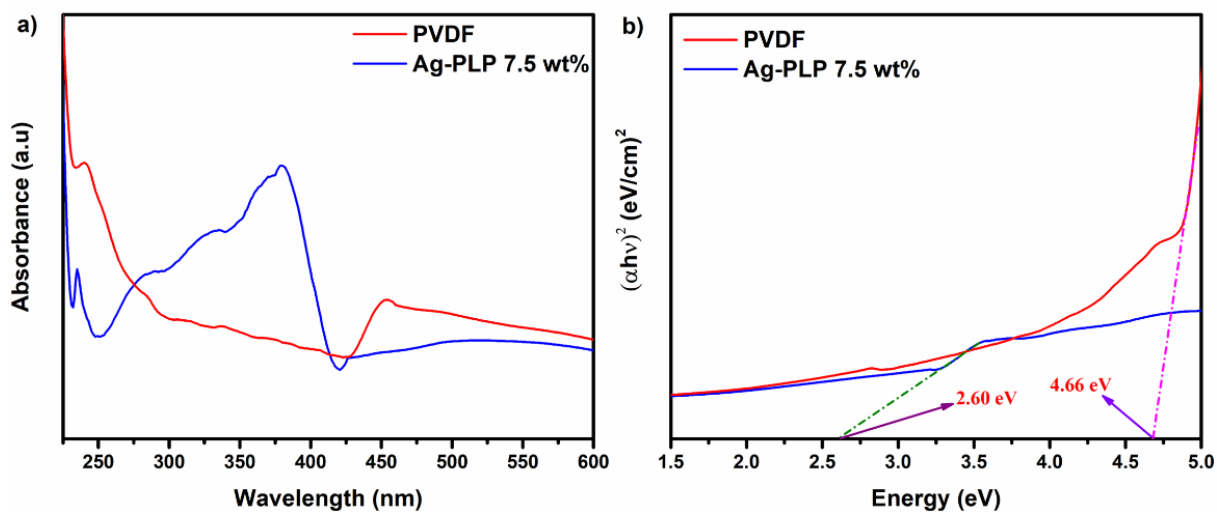

Figure 4. (a) UV-VIS-DRS absorbance spectra, and (b) Energy bandgap of PVDF and Ag-PLP 7.5 wt%

3.4   Photocatalytic degradation of CIP (Ciprofloxacin)

3.4.1 Photocatalytic study

The PLP and Ag-PLP composites (0.02 g each) were taken in 20 mL CIP solution (20 mg·L^{-1}). The entire system was put in a constant temperature oscillator for about 30 min in the dark for adsorption and then kept in the sunlight about 90 min for desorption. After degrading, the catalyst was filtered out, and the absorbance intensity of CIP was investigated by UV-Visible spectrophotometer whose maximum absorption peaks were observed at 272 nm. Within a given concentration range, the concentration of CIP solution and its absorbance follow a linear relationship. The percentage of degrading efficiency of CIP solution can be calculated by the following Equation (4):

$$Efficiency\ (\%)\ =\ \{(C_0-C)/C_0\} \times 100 \qquad (4)$$

Where C_0 is the initial concentration, and C is the final concentration of CIP after the reaction. Adsorption-desorption equilibrium experiments were performed to determine the optimal period for the photocatalytic process, as shown in Figure 5(a). According to the results of the experiment, the highest adsorption of CIP was seen at around 272 nm. As the time passes from 15 min to 90 min, the absorbance steadily decreases. The experiment clearly shows that 90 min is the optimum time for the photocatalytic activity. Adsorption of drugs is a crucial phenomenon for photocatalytic degradation because greater adsorption means more photocatalytic degradation.

The effect of pH on CIP photodegradation by PLP and Ag-PLP composites was investigated by calculating the percentage of photo-degradation at various pH levels. As shown in Figure 5(b) the photo-degradation efficiency of the composite for CIP is best at pH=6. CIP, on the other hand, has pKa values (pK$_{a1}$=6.1, pK$_{a2}$=8.2) (Scheme 1), hence its ionisation is significantly reliant on pH. The point of zero charge (PZC) of Ag-PLP 7.5 wt% was determined to be 8.51 (Figure 5(c)). The surface was positive charged when pH<PZC, and negatively charged when pH>PZC. Because the surface is positively charged, there is a stronger attraction between the catalyst and the substrate, which improves the adsorption of CIP onto the surface of the catalyst and hence the degrading efficiency.
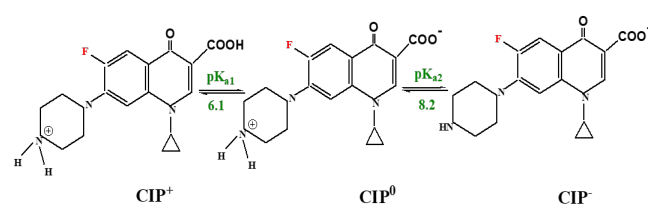
The photocatalytic degradation of all the catalysts were evaluated in presence of sun light at pH=6 for 90 min. The photocatalytic degradation percentage of different synthesized polymer samples are shown in Figure 5(d-e). Due to the effect of increase in weight percentage of LSMO ceramic, the optimised PL 5.0 wt% was doped with different weight percentage of PANI and observed that the percentage degradation increases in PLP (about 51%) with the effect of increase in weight percentage of PANI. Similarly, the effect of addition of silver, increased the degradation percentage (about 82%) in Ag-PLP and decreased at higher loading of Ag, i.e., Ag-PLP 10.0 wt%. All of the Ag loaded photocatalysts performed better than pure PLP due to the surface plasmon resonance effect, which increases photo-reduction efficiency by extending light absorption to the UV-Visible light band. In comparison to other Ag loaded photocatalysts, Ag-PLP 7.5 wt% had the best photo-reduction efficiency with an 82.0% reduction. Therefore, Ag-PLP 7.5 wt% is used as an example to determine the photodegradation performance of the composite for CIP.

The rate of photodegradation reduced as CIP concentration increased. This experimental data is consistent with the graph of the first order kinetics expressed in Equation (5):

$$Log\ C/C_0\ =\ kt \qquad (5)$$

Where C is the concentration after degradation and C_0 is initial concentration of CIP. The rate constant of a pseudo-first-order kinetics reaction is represented by K. The photodegradation of CIP was evaluated by taking all the photocatalysts as shown in Figure 5(f). The effect of CIP concentration on photodegradation of CIP in the presence of sunlight was investigated. The photodegradation vs time graph shows that increasing the CIP level from 20 mg·L^{-1} to 80 mg·L^{-1} reduced photodegradation efficiency. This is most likely due to a rise in CIP, which effects solar absorption, reducing light utilisation by Ag to some extent.

Several scavenging agents, including PBQ, IP, CA and DMSO are used to trap the potential active radicals O$_2$$^-$, OH$\cdot$, h$^+$ and e$^-$ respectively. The experiment shows that the addition of CA considerably reduced the photodegradation of CIP. This confirmed that h$^+$ is the active species involved in the photodegradation process. Figure 5(g) shows the impact of several scavenging agents on the photodegradation process. After every photocatalytic experiment, the composite was dried and washed with water and anhydrous ethanol to assess its reusability. The photodegradation efficiency does not significantly drop after four consecutive cycles, as seen in Figure 5(h), suggesting that Ag-PLP 7.5 wt% composite is stable during photocatalysis. The Figure 5(i) represents the X-ray diffraction (XRD) reflection of before and after degradation of Ag-PLP 7.5 wt% polymer composite. The diffraction patterns of composite films were obtained by Rigaku X-ray diffractometer using CuK$_\alpha$ (λ = 1.54056 Å) mono-chromatic radiation (10°$\leq$2$\theta$$\leq$80°). The highest intensity peaks were matched with the phase lanthanum strontium manganese oxide (LSMO) whose diffraction peaks to be found at 2θ values of 32.88 (320), 44.20 (52-1), 58.64 (90-1) and 59.84 (04-1) having reference ID: 00-054-1219. Some less intensity peaks are also observed which are matched with the impurity phase and diffraction peaks to be found at 2θ values of 25.18 (101), 25.81 (11-1), 35.17 (021), 36.13 (311) and 43.18 (321) having reference ID: 01-084-1778. The diffraction peak appeared around 2θ=41.02 corresponding to the presence of Ag [25]. A broad peak occurred at 2θ=25.53 which shows the amorphous nature of PANI [26,27]. All the above results demonstrated that silver, PANI, LSMO all are successfully doped into PVDF membranes. The results also suggested that the intensity of the Ag-PLP 7.5 wt% becomes relatively low after its fourth usage which may be due to the photo corrosion and photo dissolution of the catalyst.

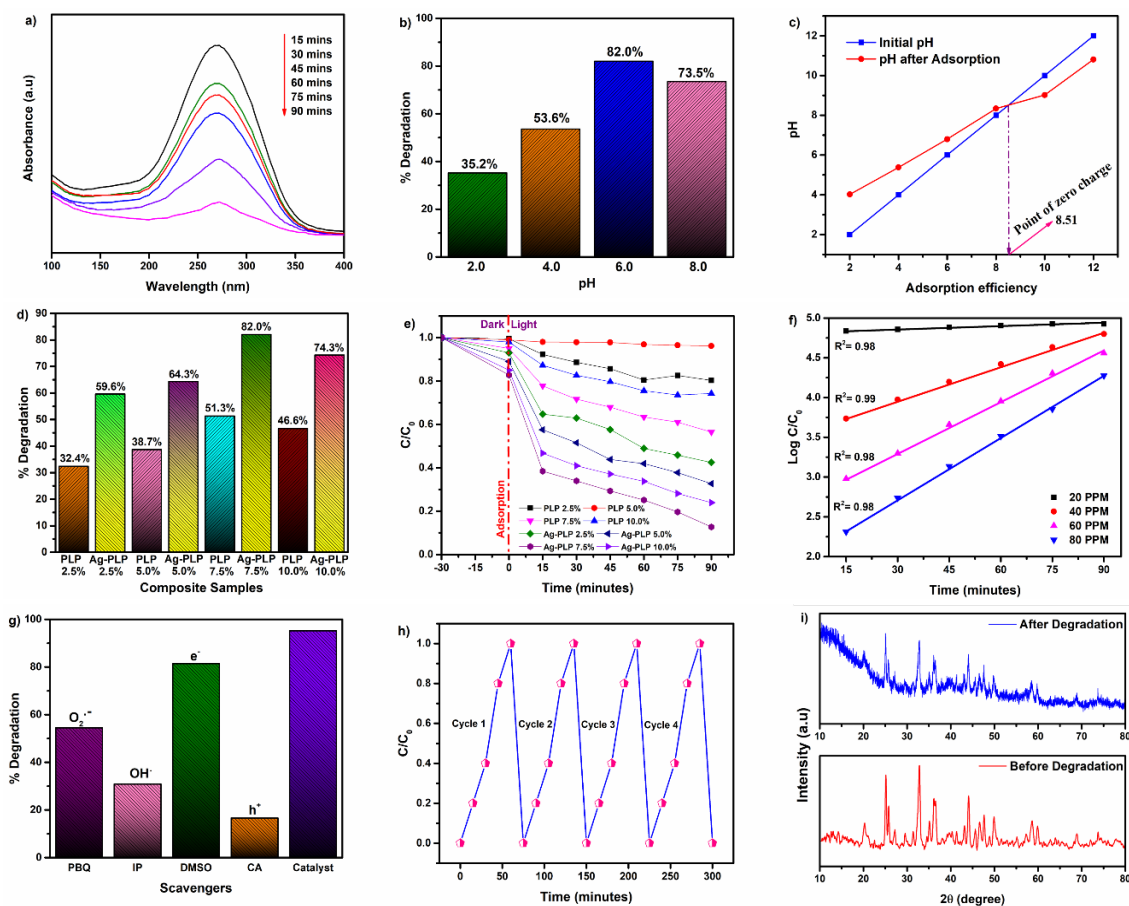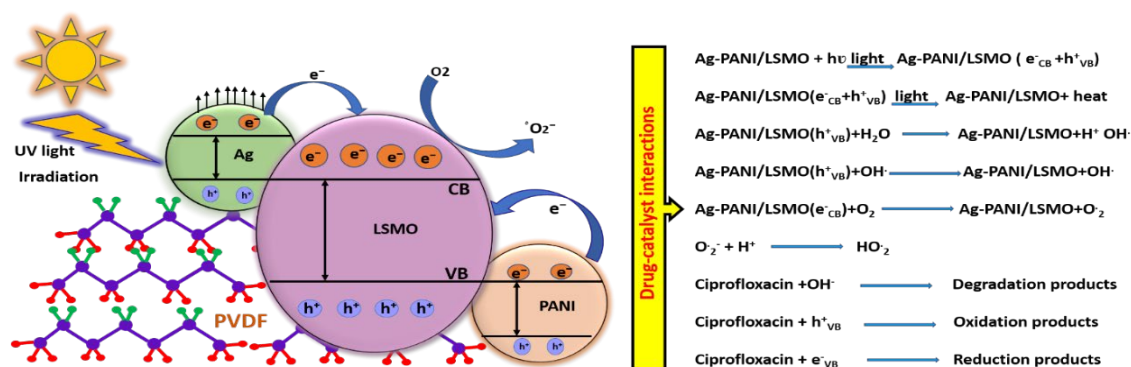**Scheme 1.** Increasing of pH caused different form of CIP.

Figure 5. (a) Photodegradation of CIP by Ag-PLP 7.5% at different time intervals, (b) Photodegradation of CIP by Ag-PLP 7.5% at different pH, (c) Point of zero charge (PZC) of Ag-PLP 7.5%, (d) Best Photocatalyst, (e) Photodegradation of CIP by various composite at different time, (f) Pseudo-first order kinetics at different concentration, (g) Impact of several scavenging agents on the photodegradation process, (h) Reusability, and (i) XRD reflection of before and after degradation of Ag-PLP 7.5%.
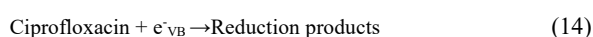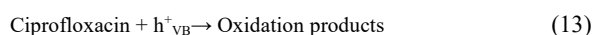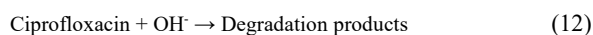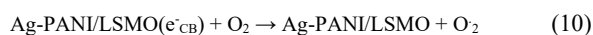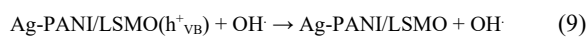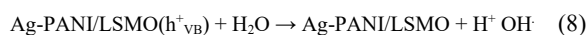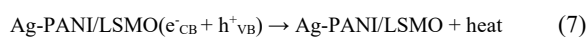

Scheme 2. Schematic diagram for possible photocatalytic mechanism of Ag-PLP photocatalyst.

3.4.2 Photocatalytic mechanism

The alteration of Ag on the surface of PLP improves photoreduction efficiency due to the surface of plasmon effect. The two most significant photocatalytic processes are the formation and separation of photoexcited electron hole pairs and a potential photocatalytic mechanism of charge transfer in Ag-PLP. There are three approaches to improve the solar driven photocatalysis as the Ag modification occurs on the PLP surface: (i) the process known as "plasmon-induced resonance energy transfer"

[28] through which the plasmon in Ag can transmit energy to PLP resulting in electron-hole pairs; (ii) the induced hot electrons that are generated by LSPR (located surface plasmon resonance) [29] shift to PLP, increasing the number of free electrons in PLP; (iii) the separation of e⁻ hole pairs occurs for which the photogenerated e⁻s in PLP migrating to Ag due to the reduced work function. The photocatalytic process for degradation of CIP was shown in Scheme 2 and following reactions (Equation (6-14)) occur during this photocatalytic process:

$$Ag\text{-}PANI/LSMO + h\upsilon \rightarrow Ag\text{-}PANI/LSMO\ (e^-_{CB} + h^+_{VB}) \qquad (6)$$

$$Ag\text{-}PANI/LSMO(e^-_{CB} + h^+_{VB}) \rightarrow Ag\text{-}PANI/LSMO + heat \qquad (7)$$

$$Ag\text{-}PANI/LSMO(h^+_{VB}) + H_2O \rightarrow Ag\text{-}PANI/LSMO + H^+\ OH^- \qquad (8)$$

$$Ag\text{-}PANI/LSMO(h^+_{VB}) + OH^- \rightarrow Ag\text{-}PANI/LSMO + OH^- \qquad (9)$$

$$Ag\text{-}PANI/LSMO(e^-_{CB}) + O_2 \rightarrow Ag\text{-}PANI/LSMO + O^-_2 \qquad (10)$$

$$O^-_2 + H^+ \rightarrow HO_2 \qquad (11)$$

$$Ciprofloxacin + OH^- \rightarrow Degradation\ products \qquad (12)$$

$$Ciprofloxacin + h^+_{VB} \rightarrow Oxidation\ products \qquad (13)$$

$$Ciprofloxacin + e^-_{VB} \rightarrow Reduction\ products \qquad (14)$$

4. Conclusion

The present communication explained successfully (I) the effect of PANI in the PVDF-LSMO-PANI composites towards the photo-catalytic degradation of ciprofloxacin drug and (II) the effect of Ag doping in the Ag-PVDF-LSMO-PANI composites towards the photo-catalytic degradation of ciprofloxacin drug. It is now evident that the incorporation of PANI in PVDF-LSMO and Ag in PVDF-LSMO-PANI polymer ceramic composites can improve the photocatalytic degradation of ciprofloxacin in the visible range of electromagnetic radiation. The presences of Ag and the ceramic phase could be verified from the XRD diffraction pattern before and after degradation of Ag-PLP 7.5%. A remarkable amount of photocatalytic activity is potentially shown in the synthesized Ag-PLP composites. The separation of photogenerated electron hole pairs (e⁻and h⁺) carried on by charge migration was mostly attributed to the improved photocatalytic activity of Ag-PLP composites. A potential photo-catalytic process for drug reduction was brought up over Ag-PLP composite. The CIP removal efficiency of Ag-PLP was 82.0% which showed higher than the unmodified LSMO in UV-Visible light irradiation at the experimental conditions. The photocatalytic properties of the Ag doped PLP composite material allow it to degrade ciprofloxacin under visible light, which is a significant advantage over other photocatalysts that require UV light.

Overall, the Ag doped PLP composite material has the potential to revolutionize the field of wastewater treatment by providing an effective and efficient method for the degradation of ciprofloxacin and other pharmaceutical drugs. Its impact extends beyond the scientific community, as it contributes to the improvement of public health and the protection of the environment.

Authorship contribution

Swayam Aryam Behera: Methodology, Investigation, Formal analysis, Data curation, Writing - original draft;

Ali Amanat: Formal analysis, Data curation;

P. Ganga Raju Achary: Conceptualization, Validation, Editing, Review and revision.

Declaration

The authors declare that there is no conflict of interest for this manuscript.

Reference

[1] P. M. Rajaitha, S. Hajra, M. Sahu, K. Mistewicz, B. Toron, R. Abolhassani, S. Pando, Y. K. Mishra, and H. J. Kim, "Unraveling highly efficient nanomaterial photocatalyst for pollutant removal: a comprehensive review and future progress," *Materials Today Chemistry*, vol. 23, p. 100692, 2022.

[2] K. Wirandorn, N. Panyayao, and V. Siriwongrungson, "Characterization and photocatalytic activity of titanium dioxide deposited on stainless steel by pulsed-pressure MOCVD," *Journal of Metals, Materials and Minerals*, vol. 28, no. 2, 2018.

[3] P. Norranattrakul, K. Siralertmukul, and R. Nuisin, "Fabrication of chitosan/titanium dioxide composites film for the photocatalytic degradation of dye," *Journal of Metals, Materials and Minerals.*, vol. 23, no. 2, 2013.

[4] J. Swain, A. Priyadarshini, S. Hajra, S. Panda, J. Panda, R. Samantaray, Y. Yamauchi, M. Han, H. J. Kim, and R. Sahu, "Photocatalytic dye degradation by BaTiO3/zeolitic imidazolate framework composite," *Journal of Alloys and Compounds*, vol. 965, p. 171438, 2023.

[5] S. Saha, R. P. Singh, A. Rout, A. Mishra, A. Ali, H. Basumatary, and R. Ranjan ,"Inducing ferromagnetism and magnetoelectric coupling in the ferroelectric alloy system BiFeO₃--PbTiO₃ via additives," *Journal of Applied Physics*, vol. 133, no. 6, 2023.

[6] H. Wang, J. Li, P. Huo, Y. Yan, and Q. Guan, "Preparation of Ag₂O/Ag₂CO₃/MWNTs composite photocatalysts for enhancement of ciprofloxacin degradation," *Applied Surface Science*, vol. 366, pp. 1-8, 2016.

[7] N. R. Alluri, B. Saravanakumar, and S.-J. Kim, "Flexible, hybrid piezoelectric film (BaTi ₍₁₋ₓ₎ Zr ₓ O₃)/PVDF nanogenerator as a self-powered fluid velocity sensor," *ACS Applied Materials & interfaces*, vol. 7, no. 18, pp. 9831-9840, 2015.

[8] Y. Zhang, Y. Zhang, X. Xue, C. Cui, B. He, Y. Nie, P. Deng, and Z. L. Wang, "PVDF--PZT nanocomposite film based self-charging power cell," *Nanotechnology*, vol. 25, no. 10, p. 105401, 2014.

[9] D. Olmos, G. González-Gaitano, A. L. Kholkin, and J. González-Benito, "Flexible PVDF-BaTiO₃ nanocomposites as potential materials for pressure sensors," *Ferroelectrics*, vol. 447, no. 1, pp. 9-18, 2013.

[10] J. Prokeš, and J. Stejskal, "Polyaniline prepared in the presence of various acids: 2. Thermal stability of conductivity," *Polymer Degradation and Stability*, vol. 86, no. 1, pp. 187-195, 2004.

[11] P. K. Kahol, K. K. S. Kumar, S. Geetha, and D. C. Trivedi, "Effect of dopants on electron localization length in polyaniline," *Synthetic Metals*, vol. 139, no. 2, pp. 191-200, 2003.

[12] F. Davodi, M. Tavakkoli, J. Lahtinen, and T. Kallio, "Straightforward synthesis of nitrogen-doped carbon nanotubes as highly active bifunctional electrocatalysts for full water splitting," *Journal of Catalysis*, vol. 353, pp. 19-27, 2017.

[13] T. Rasheed, M. Bilal, F. Nabeel, M. Adeel, and H. M. N. Iqbal, "Environmentally-related contaminants of high concern: potential sources and analytical modalities for detection, quantification, and treatment," *Environment International,* vol. 122, pp. 52-66, 2019.

[14] A. K. Al-Buriahi, M. M. Al-shaibani, R. M. S. R. Mohamed, A. A. Al-Gheethi, A. Sharma, and N. Ismail, "Ciprofloxacin removal from non-clinical environment: A critical review of current methods and future trend prospects," *Journal of Water Process Engineering*, vol. 47, p. 102725, 2022.

[15] M. Danish, L. L. Estralla, I. M. A. Alemaida, A. Lisin, N. Moiseev, M. Ahmadi, M. Nazari, M. Wali, H. Zaheb, and T. Senjyu, "Photocatalytic applications of metal oxides for sustainable environmental remediation," *Metals (Basel).*, vol. 11, no. 1, p. 80, 2021.

[16] P. G. R. Achary, P. Pattanaik, and B. Nanda, "Facile synthesis of lanthanum doped strontium manganite for photocatalytic decolourization of malachite green," *Inorganic Chemistry Communications.*, vol. 158, p. 111545, 2023.

[17] X. Du, Y. Xu, L. Xiong, Y. Bai, J. Zhu, and S. Mao, "Polyaniline with high crystallinity degree: Synthesis, structure, and electrochemical properties," *Journal of Applied Polymer Science,* vol. 131, no. 19, 2014.

[18] A. N. Jarad, K. Ibrahim, and N. M. Ahmed, "Synthesis and characterization thin films of conductive polymer (PANI) for optoelectronic device application," in *AIP Conference Proceedings*, 2016, vol. 1733, no. 1, p. 20020.

[19] J. Coates, "Interpretation of infrared spectra, a practical approach." 2000.

[20] P. A. Tamirisa, Kn. C. Liddell, P. D. Pedrow, and M. A. Osman, "Pulsed-plasma-polymerized aniline thin films," *Journal of Applied Polymer Science*, vol. 93, no. 3, pp. 1317-1325, 2004.

[21] T. Ohsaka, Y. Ohnuki, N. Oyama, G. Katagiri, and K. Kamisako, "IR absorption spectroscopic identification of electroactive and electroinactive polyaniline films prepared by the electrochemical polymerization of aniline," *Journal of Electroanalytical Chemistry and Interfacial Electrochemistry,* vol. 161, no. 2, pp. 399-405, 1984.

[22] R. gregorio jr and M. cestari, "Phase content and morphology of poly (vinylidene fluoride)".

[23] A. Abulizi, K. Kadeer, H. Maimaitizi, Y. Tursun, and D. Talifu, "In situ ultrasound-assisted ion exchange synthesis of sphere-like $AgCl_xBr_{1-x}$ composites with enhanced photocatalytic activity and stability," *Environmental Science and Pollution Research*, vol. 27, pp. 43615-43624, 2020.

[24] M. Sharma, J. K. Quamara, and A. Gaur, "Behaviour of multiphase PVDF in (1-x) PVDF/(x) $BaTiO_3$ nanocomposite films: structural, optical, dielectric and ferroelectric properties," *Journal of Materials Sciecnce: Materials in Electronics*, vol. 29, pp. 10875-10884, 2018.

[25] Y. Lu, Y. Ma, T. Yang, and J. Guo, "Hydrophilic modification of PVDF membranes by in situ synthesis of nano-Ag with nano-ZrO_2," *Green Processing and Synthesis*, vol. 10, no. 1, pp. 538-546, 2021.

[26] S. Sathiyanarayanan, S. S. Azim, and G. Venkatachari, "Preparation of polyaniline--Fe_2O_3 composite and its anti-corrosion performance," *Synthetic Metals,* vol. 157, no. 18-20, pp. 751–757, 2007.

[27] S. M. Ambalagi, M. Devendrappa, S. Nagaraja, and B. Sannakki, "Dielectric properties of PANI/CuO nanocomposites," in *IOP Conference Series: Materials Science and Engineering*, 2018, vol. 310, no. 1, p. 12081.

[28] J. Li, S. K. Cushing, F. Meng, T. R. Senty, A. D. Bristow, and N. Wu, "Plasmon-induced resonance energy transfer for solar energy conversion," *Nature Photonics,* vol. 9, no. 9, pp. 601-607, 2015.

[29] K. A. Willets, and R. P. Van Duyne, "Localized surface plasmon resonance spectroscopy and sensing," *Annual Reviews of Physical Chemistry*, vol. 58, pp. 267-297, 2007.